

KEK-preprint-94-106
 DPNU-94-38
 NWU-HEP 94-04
 TIT-HPE-94-09
 TUAT-HEP 94-04
 OCU-HEP 94-06
 PU-94-686
 INS-REP 1051
 KOBE-HEP 94-05

$K^0(\overline{K}^0)$ Production in Two-Photon Processes at TRISTAN *

(TOPAZ Collaboration)

R.Enomoto^{a†}, K.Abe^b, T.Abe^b, I.Adachi^a, K.Adachi^c, M.Aoki^d, M.Aoki^b, S.Awa^c,
 K.Emi^e, H.Fujii^a, K.Fujii^a, T.Fujii^f, J.Fujimoto^a, K.Fujita^g, N.Fujiwara^c, H.Hayashii^c,
 B.Howell^h, N.Iida^a, R.Itoh^a, Y.Inoue^g, H.Iwasaki^a, M.Iwasaki^c, K.Kaneyuki^d,
 R.Kajikawa^b, S.Katoⁱ, S.Kawabata^a, H.Kichimi^a, M.Kobayashi^a, D.Koltick^h, I.Levine^h,
 S.Minami^d, K.Miyabayashi^b, A.Miyamoto^a, K.Muramatsu^c, K.Nagai^j, K.Nakabayashi^b,
 E.Nakano^b, O.Nitoh^e, S.Noguchi^c, A.Ochi^d, F.Ochiai^k, N.Ohishi^b, Y.Ohnishi^b,
 Y.Ohshima^d, H.Okunoⁱ, T.Okusawa^g, T.Shinohara^e, A.Sugiyama^b, S.Suzuki^b, S.Suzuki^d,
 K.Takahashi^e, T.Takahashi^g, T.Tanimori^d, T.Tauchi^a, Y.Teramoto^g, N.Toomi^c,
 T.Tsukamoto^a, O.Tsumura^e, S.Uno^a, T.Watanabe^d, Y.Watanabe^d, A.Yamaguchi^c,
 A.Yamamoto^a, and M.Yamauchi^a

^aKEK, National Laboratory for High Energy Physics, Ibaraki-ken 305, Japan

^bDepartment of Physics, Nagoya University, Nagoya 464, Japan

^cDepartment of Physics, Nara Women's University, Nara 630, Japan

^dDepartment of Physics, Tokyo Institute of Technology, Tokyo 152, Japan

^eDept. of Appl. Phys., Tokyo Univ. of Agriculture and Technology, Tokyo 184, Japan

^fDepartment of Physics, University of Tokyo, Tokyo 113, Japan

^gDepartment of Physics, Osaka City University, Osaka 558, Japan

^hDepartment of Physics, Purdue University, West Lafayette, IN 47907, USA

ⁱInstitute for Nuclear Study, University of Tokyo, Tanashi, Tokyo 188, Japan

^jThe Graduate School of Science and Technology, Kobe University, Kobe 657, Japan

^kFaculty of Liberal Arts, Tezukayama University, Nara 631, Japan

* to be published in Phys. Lett. **B**.

†Internet address: enomoto@kekvox.kek.jp.

Abstract

We have carried out an inclusive measurement of $K^0(\overline{K}^0)$ production in two-photon processes at TRISTAN. The mean \sqrt{s} was 58 GeV and the integrated luminosity was 199 pb⁻¹. High-statistics K_s samples were obtained under such conditions as no-, anti-electron, and remnant-jet tags. The remnant-jet tag, in particular, allowed us, for the first time, to measure the cross sections separately for the resolved-photon and direct processes.

1 Introduction

Excess over theoretical predictions was reported in references [1, 2], concerning charm pair production in two-photon processes. These references extensively discussed possibilities to explain the excess by increasing the predicted cross sections of two-photon processes. In order to help sorting out these possibilities, we have carried out an inclusive measurement of $K^0(\overline{K}^0)$ mesons in two-photon processes. With the point-like process (direct process [3]) where $e^+e^- \rightarrow e^+e^-s\bar{s}$ is strongly suppressed due to the small value of Q_s^4 (Q_s is s quark's charge), K_s 's, particularly in the high- P_T region, come mainly from $c\bar{c}$ production [4]. The use of K_s 's also enhances the sensitivity to two-photon processes at low P_T .

There are additional advantages in this K_s analysis, which are high statistics and low systematics, thanks to high acceptance and use of only a central tracking device, respectively. Moreover, using the low angle calorimeter [5], we could obtain the cross section for the resolved photon process [6] separately. We can thus test some of the possibilities suggested in reference [2]: we proposed to use a low charm quark mass (1.3 GeV), the next-to-leading-order correction (NLO), and the intrinsic parton P_T inside photon in order to explain an excess observed in the $c\bar{c}$ cross section especially in the high- P_T region.

Notice also that this analysis is hardly affected by \tilde{t} (superpartner of the top quark) pair production [7] discussed in references [1, 2], even if present, since the high- Q^2 decay of $c \rightarrow \overline{K}^0 X$ smears the P_T distribution of the K_s 's and thus diminishes the sensitivity to the \tilde{t} pair production.

2 Event selection

The data used in this analysis were obtained with the TOPAZ detector at the TRISTAN e^+e^- collider, KEK[8, 9]. The mean \sqrt{s} was 58 GeV and the integrated luminosity was 199 pb^{-1} . A forward calorimeter (FCL), which covered $0.98 < |\cos \theta| < 0.998$ (θ is the polar angle, i.e., the angle with respect to the electron beam), was installed in the course of the experiment. The FCL was made of bismuth germanate crystals (BGO), and was used to anti-tag the beam electrons (positrons) and to tag hadrons (remnant-jets) [5] for this study. We could thus select collisions of almost-real photons including resolved photon processes[6]. The integrated luminosity of the data with the FCL detector was 175 pb^{-1} .

A description of our trigger system can be found in reference [10]. The requirement for the charged track trigger was two or more tracks with an opening angle of greater than 45-90 degrees. The P_T threshold for charged particles was 0.3-0.7 GeV, varied depending on beam conditions.

The event selection criteria were as follows: three or more charged particles ($P_T > 0.15 \text{ GeV}$, $|\cos \theta| < 0.77$), the invariant mass (W_{VIS}) of visible particles ($|\cos \theta| < 0.77$) had to be greater than 2 GeV, the event-vertex position had to be consistent with the interaction point, and the visible energy had to be less than 25 GeV. In total, 220378 events were selected.

3 Monte-Carlo simulation

In order to estimate the acceptances and backgrounds in this analysis, we used the following Monte-Carlo simulation programs. For the generation of single-photon-exchange hadronic events, we used JETSET6.3[11] with the parameter values given in reference

[12]. Details concerning the event generation of direct as well as resolved-photon and vector meson dominance (VDM) processes can be found in references [1, 2, 14]. Here, we just note the following points. For $c\bar{c}$ generation, we used the current charm quark mass of 1.3 GeV to calculate cross sections for point-like processes and a constituent charm quark mass of 1.6 GeV for hadronization procedure, and made the next-to-leading order (NLO) correction, whose details can be found in references [1, 2, 15]. Light-quark generation was carried out by using the lowest order (LO) formula with a P_T^{min} cut of 2.5 GeV. We used the parton density functions by Levy-Abramowicz-Charchula set-1 (LAC1) [16] for the resolved-photon process. Generated events were processed through the standard TOPAZ detector simulation program [12], in which hadron showers were simulated with an extended version of GHEISHA 7 [13]. Its data on hadron interactions with nuclei had been updated to fit various experimental cross sections.

Using the above-mentioned Monte-Carlo simulations, the trigger efficiency for the sum of the direct and resolved photon processes was estimated to be 79%, 97% of which represented charged trigger events. The event-selection efficiency after the trigger was obtained to be 80%.

4 Tagging conditions

The tagging conditions were as follows. For anti-electron tagging, there had to be no energy deposit of more than $0.4E_b$ in $|\cos\theta| < 0.998$ (anti-electron tag or anti-tag), where E_b is the beam energy. This selected events from collisions of almost real photons, for which the accuracy of the equivalent photon approximation was expected to be reliable at the 1% level. When the energy cut was lowered, mis-anti-tag due to beam remnant hadrons (remnant-jets) became significant, as predicted by the Monte-Carlo simulations. The energy distribution of the maximum-energy cluster in FCL is shown in Figure 1.

The horizontal scale is normalized at the beam energy. The Monte-Carlo predictions for single-photon-exchange, VDM, and resolved-photon processes are shown by histograms. The peak around 1 was explained by the direct processes. This implies a possibility to tag the resolved photon process by requiring, for instance, $500 \text{ MeV} < E_{FCL} < 0.25 E_b$, where E_{FCL} is the energy deposit in the FCL (remnant-jet tag or rem-tag). We did not use any hadron shape information because of large segmentation and lack of tracking information. The yield of the remnant-jet tag events agreed with our Monte-Carlo simulation within 5% level. Our analysis is the first trial that uses this tag. An event selection without these two tags is called, hereafter, “no-electron tag” or “no-tag”. The fractions of electron and remnant-jet tag events to no-tag ones were obtained to be 2.4 and 47% of the selected events, respectively.

In the Monte-Carlo simulations, we used the equivalent photon approximation with the photon flux expression given in reference [17]. We set the Q_γ^2 limit at the smaller of $P_{T,q}^2 + m_q^2$ and the anti-tag limit $[2E_b^2(1-x_\gamma)(1-\cos\theta_{max}) : x_\gamma = 0.4, \theta_{max} = 3.2 \text{ degrees}]$, where $P_{T,q}$ and m_q are the transverse momentum and the mass of a quark, respectively [18].

The tagging efficiency of the remnant-jet tag for the resolved photon process was estimated to be 72% without assuming FCL noise which will be described later. We tried two ways of generating remnant partons: one along the beam direction, and the other using a Gaussian distribution of P_T -width 0.44 GeV with respect to the beam axis. Two methods differed in acceptance only by 3%. On the other hand, the tagging efficiency of the remnant-jet tag for the direct process was estimated to be 10.8% without assuming FCL noise.

5 Analysis

The charged-track selection criteria for the K_s analysis were as follows: for each track P_T had to be greater than 0.15 GeV, dE/dx had to be consistent with the pion assumption ($\chi^2_{\pi^\pm} < 10$), $|\cos\theta|$ had to be less than 0.77, and the closest approach to the interaction point in the XY-plane (perpendicular to the beam axis) had to be greater than 1 cm. Using these selected tracks, we looked for opposite-sign pairs with an opening angle less than 90 degrees, and carried out secondary vertex reconstructions three-dimensionally. Finally, we demanded these pairs to be consistent with the assumption that they came from the event vertices with a flight length larger than 3 cm. The invariant-mass distributions of these candidate $\pi^+\pi^-$ pairs are plotted in Figure 2 for the three tagging conditions, respectively. These invariant-mass spectra were fitted with the sum of a second-order polynomial and a Gaussian distribution and the peak entries were obtained for no-, remnant-jet, and electron tags to be 893 ± 34 , 364 ± 22 , and 75.8 ± 9.5 K_s 's, respectively. The peak position and the width were consistent with the detector simulation. In order to derive the differential P_T cross sections, we divided P_T into ten bins, as shown in Table 1. Notice that even the lowest-statistics bin gave a 5.1- σ K_s peak (in the no-electron tag case).

6 Background subtractions

Single-photon-exchange process was a largest background especially for high- P_T K_s . This can be reduced when a cut was applied on the total visible energy. We, however, did not carry out this, because we did not want to reduce the acceptance for high- P_T K_s . The contamination from the single-photon-exchange process was estimated and subtracted using the Monte-Carlo simulation, on a bin by bin basis. The background fractions for no-tag were 6.0, 6.1, 6.5, 8.1, 10.0, 11.0, 14.3, 17.3, 43.4, and 48.1%, respectively, for the

P_T bins shown in Table 1, being strongly P_T dependent. We estimated these fractions for anti- and remnant-jet tags. They were consistent with the above values within statistical errors. The background from beam gas interactions was estimated using the off-vertex events in the beam direction: there was a vacuum leak in the beam pipe for some period. The beam gas contribution for no-tag was 7.8% on the average, and was subtracted from the data. For anti- and remnant-jet tags, the above value became slightly large (9.8%), i.e., electron-tag sample was free from the beam-gas background. FCL noise hits were studied by analysing random trigger and Bhabha events. The probability of noise hits with $E_{FCL} > 0.5$ GeV was estimated to be 12.1%, while for hits with $E_{FCL} > 0.4E_b$, it reduces to 0.1%. The FCL noise was also related to the vacuum leak. In the Monte-Carlo simulations, we added noise hits randomly in accordance with the observed noise hit probability in order to reliably estimate the tagging efficiencies. Using this, the tagging efficiencies of the remnant-jet tag for the resolved-photon and direct processes were estimated to be 75% and 21%, respectively.

7 Systematic errors

The systematic errors were estimated, bin by bin, as follows. For the trigger, we added some extra noise hits in the tracking chambers in the simulations. For the event selection and the K_s reconstruction, we changed the cut values and evaluated systematic errors as the cross-section differences. We also changed the pulse-height threshold in the TPC simulation to evaluate the effects on its tracking efficiency. We added the obtained systematic errors quadratically, on a bin by bin basis. The average over the P_T bins of the systematic errors was 12%, of which the cut dependence in the event selection was the dominant source. These systematic errors were quadratically added to statistical errors. We also checked the acceptance ambiguity due to the parametrization dependence of

the resolved-photon processes, by comparing the LAC1 [16] and Drees-Grassie [DG] [19] parametrizations. The acceptance difference was estimated to be 5.9%, which is small compared to the systematic errors shown above.

8 Results

The P_T differential cross sections were obtained from the number of reconstructed K_s 's in each bin and its corresponding efficiency estimated with the Monte-Carlo simulations described previously. They are listed in Table 1 and plotted in Figures 3 (a) - (e) for the three tagging conditions and two subtraction schemes, respectively. Figure 3 (a) is for anti-electron tag events. In the remnant-jet tag events, the Monte-Carlo simulation predicted a significant contamination from VDM events. The tagging efficiency for the VDM process was estimated to be $\sim 61\%$, slightly smaller than that of the resolved-photon process. In addition there was a large ambiguity in the cross section of the VDM process. Therefore we calculated the cross sections using two subtraction schemes. Figures 3 (b) and (e) were obtained by subtracting the VDM contribution predicted by the Monte-Carlo simulation (VDM subtraction) for remnant-jet and anti-remnant-jet tags, respectively. Here, the “anti-remnant-jet tag” cross section was obtained by subtracting the remnant-jet tag cross section from that of the anti-electron tag. Figures 3 (c) and (d) were obtained without the VDM subtraction. In Figures 3 (b) and (d), the contribution of the direct process was subtracted, since the uncertainty in the prediction of this process was considered to be small. The histograms in Figures 3 (a) - (e) are the Monte-Carlo predictions: the cross-hatched, singly-hatched, and open areas are predictions for the direct, resolved-photon (LAC1), and VDM processes.

9 Discussions

The fraction of charm events was studied using the above-mentioned Monte-Carlo simulations. We found 55% of these events with $P_T(K_s) > 1.4$ GeV were of charm origin. On the other hand, only 30% of the events with charged tracks of $P_T > 1.4$ GeV were from $c\bar{c}$ pairs. Also, the Monte-Carlo simulations predicted that 70% of these high- P_T charm events originated from the direct process. In this study, we derived six types of cross sections using different tagging conditions and subtraction schemes. We can therefore separately compare each cross section with the theoretical prediction for each process.

Firstly, about 30% of the high- P_T events can be explained as the electron-tagged events (see Table 1). Secondly, for the anti-tag cross section [Figure 3 (a)], the agreement, especially in the lower- P_T region, is reasonably good, considering the ambiguities due to the VDM process. They are, however, higher than the theoretical predictions in the high- P_T region ($P_T > 1.2$ GeV) by 2.2σ .

The cross section with the anti-remnant-jet tag is consistent with the predictions of the direct and VDM processes [Figures 3 (c) and (e)]. The hypothetical \tilde{t} pair production with $m_{\tilde{t}}=15$ and $m_{\tilde{\gamma}}=12.7$ GeV [1, 2] is expected to increase these cross sections by 1.7, 1.1, and 0.3 pb/GeV in the highest three P_T bins, respectively, which are smaller than the experimental errors. Therefore we could not discuss this hypothesis by this analysis result. Note also that this hypothesis turned out to be inconsistent with the recent search by the VENUS collaboration [20].

The dominant source of the discrepancy lies in Figures 3 (b) and (d), i.e., in the remnant-jet tag sample (we considered that this sample was dominated by the resolved-photon and/or VDM processes): the spectrum looks harder than the prediction of the resolved photon process. The histograms in Figures 3 (b) and (d) have already been

corrected by the NLO factor ($0.5P_{T,c}+0.54$; $P_{T,c}$ is a P_T of a charm quark) [1, 2, 15]. This factor, which is due to the presence of off-shell gluon emissions from resolved quarks, is large especially in the high P_T region. The measured spectrum is harder than the LO prediction, and is close to the spectrum of the direct process. Our data suggest the importance of the NLO correction. The NLO correction to the light quark events, which is absent from our present Monte-Carlo generator, is also considered to be necessary. In addition, the intrinsic parton P_T (we used 0.44 GeV with a Gaussian distribution) is necessary. In summary, the theoretical prediction agrees with our data to a reasonably good accuracy, justifying our parametrization of the Monte-Carlo generation.

In order to check if the parton density functions have anything to do with the discrepancy, we compared our remnant-jet-tag data [Figure 3 (d)] with the predictions from six sets of parametrizations by Hagiwara, Tanaka, Watanabe, and Izubuchi [WHIT1-6] [18]. A systematic analysis on gluon distributions can be carried out using these parametrizations. The results are shown in Figures 4 (a) and (b), where the histograms are the predictions by the WHIT 1-6 parametrizations with P_T^{min} 's of 2.0 and 2.5 GeV. Notice that the predictions are rather sensitive to the P_T^{min} cut and the VDM contribution, especially in the low- P_T region; $P_T < 1$ GeV. There are some possible combinations which reproduce the high- P_T cross sections well. It is, however, necessary to improve the prediction of the VDM process.

10 Conclusion

We carried out an inclusive measurement of $K^0(\overline{K}^0)$ in two-photon processes at TRISTAN. The mean \sqrt{s} was 58 GeV and the integrated luminosity was 199 pb⁻¹. High-statistics K_s samples were obtained under such conditions as no-, anti-electron, and remnant-jet tags. Especially with the remnant-jet tagging, we could unambiguously extract the con-

tribution from the resolved photon process. Comparisons with the theoretical predictions were carried out. Our results agreed with the theoretical predictions with a low charm mass ($m_c=1.3$ GeV), intrinsic parton P_T inside photon ($\sigma_{P_T}=0.44$ GeV), and the NLO corrections, i.e., those obtained by the previous results of the $D^{*\pm}$ analysis [1, 2].

Acknowledgement

We would like to thank Prof. H. Terazawa (INS) for discussions concerning the theoretical predictions. We also thank Drs. K. Hagiwara, M. Tanaka, I. Watanabe (KEK), and Mr. T. Izubuchi (Univ. of Tokyo) for instructions on the WHIT parametrizations.

References

- [1] R. Enomoto et al., Phys. Rev. **D50**, 1879 (1994).
- [2] R. Enomoto et al., Phys. Lett. **B328**, 535 (1994).
- [3] See e.g. S. J. Brodsky, T. Kinoshita, and H. Terazawa, Phys. Rev. **D4** (1971) 1532.
- [4] D. Cords et al., Phys. Lett. **B 302**, 341 (1993).
- [5] H. Hayashii et al., Nucl. Instrum. Method., **A316** 202 (1992).
- [6] S. J. Brodsky, T. A. DeGrand, J. F. Gunion, and J. H. Weis, Phys. Rev. Lett. **41** (1978) 672; Phys. Rev. **D19** (1979) 1418; H. Terazawa, J. Phys. Soc. Japan, **47** (1979) 355; K. Kajantie and R. Raitio, Nucl. Phys. **B159** (1979) 528.
- [7] J. Ellis and S. Rudaz, Phys. Lett. **B128**, 248 (1983); E. Haber and G. L. Kane, Phys. Rep. **117**, 75 (1985); K. Hikasa and M. Kobayashi, Phys. Rev. **D 36**, 724 (1987); M. Drees and K. Hikasa, Phys. Lett. **B 252**, 127 (1990).
- [8] A. Imanishi et al., Nucl. Instrum. Methods, **A269** 513 (1988); A. Yamamoto et al., Jpn. J. Appl. Phys. Lett., **25** L440 (1986); S. Kawabata et al., Nucl. Instrum. Methods, **A270** 11 (1988); J. Fujimoto et al., Nucl. Instrum. Methods, **A256** 449 (1987); S. Noguchi et al., Nucl. Instrum. Methods, **A271** 464 (1988).
- [9] T. Kamae et al., Nucl. Instrum. Methods, **A252** 423 (1986).
- [10] R. Enomoto et al., Nucl. Instrum. Methods, **A269** 507 (1988); R. Enomoto, K. Tsukada, N. Ujiie, and A. Shirahashi, IEEE Trans. NS. **Vol. 35, No. 1**, 419 (1988); T. Tsukamoto, M. Yamauchi, and R. Enomoto, Nucl. Instrum. Meth. **A297** 148 (1990).

- [11] T. Sjöstrand, Comput. Phys. Commun., **39** (1986) 347; T. Sjöstrand and M. Bengtsson, Comput. Phys. Commun., **43** (1987) 367.
- [12] I. Adachi et al., Phys. Lett. **B227** (1989) 495.
- [13] H. Fesefeldt, Nucl. Instrum. Meth. **A 267** (1988) 367.
- [14] H. Hayashii et al., Phys. Lett. **B314** (1993) 149.
- [15] M. Drees, M. Krämer, J. Zunft, and P. M. Zerwas, Phys. Lett. **B306** (1993) 371.
- [16] H. Abramowicz, K. Charchula, and A. Levy [LAC], Phys. Lett. **B269** (1991) 458.
- [17] S. Frixione, M. L. Mangano, P. Nason, and G. Ridolfi, Phys. Lett. **B 319**, 339 (1993).
- [18] H. Hagiwara, M. Tanaka, I. Watanabe, and T. Izubuchi [WHIT], KEK Preprint 93-160, submitted for publication.
- [19] M. Drees and K. Grassie [DG], Z. Phys. **C28** (1985) 451.
- [20] J. Shirai et al., Phys. Rev. Lett. **72** (1994) 3313.

Table 1, R. Enomoto et al., Physics Letters B.

tag cond. VDM subt.	no-tag -	anti-tag -	rem-tag yes	anti-rem-tag no	rem-tag no	anti-rem-tag yes
P_T range (GeV)	cross sections (pb/GeV)					
0.3-0.55	889± 248	810± 247	43± 52	767± 247	613± 237	197± 282
0.55-0.65	839± 166	783± 168	53± 42	731± 170	520± 161	263± 202
0.65-0.75	703± 114	593± 109	99± 34	494± 108	556± 117	37± 137
0.75-0.9	415± 73	371± 70	34± 20	337± 69	241± 62	129± 74
0.9-1.05	236± 32	213± 32	41± 14	172± 33	161± 33	52± 42
1.05-1.2	162± 24	116± 22	14± 10	102± 23	51± 20	65± 28
1.2-1.4	70± 12	62± 12	16± 7	46± 14	30± 10	32± 15
1.4-1.7	37.7± 8.3	30.6± 7.6	15.8± 5.3	14.8± 8.0	19.1± 6.1	11.5± 8.3
1.7-2.5	7.2± 2.2	4.8± 2.0	4.7± 1.8	0.1± 2.5	4.8± 1.9	0.0± 2.5
2.5-5	1.78±0.73	1.63±0.70	0.98±0.64	0.65±0.93	0.98±0.64	0.65±0.93

Table 1: Differential cross section of $K^0(\overline{K}^0)$ versus P_T (GeV), $d\sigma/dP_T$ (pb/GeV), for $|\cos\theta| < 0.77$. Six cases are listed: no-tag , anti-electron tag, remnant-jet tag with VDM subtraction, anti-remnant-jet tag without VDM subtraction, remnant-jet tag without VDM subtraction, and anti-remnant-jet tag with VDM subtraction, which are described in the text.

Figure captions

Figure 1: Distribution of the energy fractions (normalized at the beam energy) of the maximum-energy clusters in FCL. The points with error bars are experimental data. The histograms are the prediction by the Monte-Carlo simulation; the cross-hatched area is single-photon-exchange process, the singly-hatched one is VDM, and the open one is resolved-photon process.

Figure 2: Invariant-mass spectra of $\pi^+\pi^-$'s. The solid histogram is for the no-electron tag, the dashed one is for the remnant-jet tag, and the dotted one is for the beam-electron tag.

Figure 3: Differential cross section of $K^0(\overline{K}^0)$ versus P_T (GeV), $d\sigma/dP_T$ (pb/GeV), for $|\cos\theta| < 0.77$. Five cases are plotted: (a) anti-electron tag, (b) remnant-jet tag with the VDM and direct process subtraction, (c) anti-remnant-jet tag without the VDM subtraction, (d) remnant-jet tag without the VDM subtraction, and (e) anti-remnant-jet tag with the VDM and direct process subtraction, as described in the text. Processes which we expected to show are; (b) resolved-photon, (c) direct and VDM, (d) VDM and resolved, and (e) direct processes. The histograms are the theoretical predictions which are described in the text. The open area is for the VDM, the singly-hatched one is for the resolved photon process, and the cross-hatched one is for the direct process.

Figure 4: Differential cross section of $K^0(\overline{K}^0)$ versus P_T (GeV), $P_T^4 d\sigma/dP_T$ (pb·GeV), for $|\cos\theta| < 0.77$ for the remnant-jet tag without the VDM subtraction. The hatched areas are the predictions by the VDM Monte-Carlo simulation. The histograms are predictions by the WHIT 1-6 parametrizations. The solid one is WHIT1, the dashed one WHIT2, the dot-dashed one WHIT3, the dotted one WHIT4, the scarce-dotted one WHIT5, and the short-dashed one WHIT6. Two values of P_T^{min} 's were used, i.e., (a) 2.0 and (b) 2.5 GeV.

Figure 1, R. Enomoto et al., Physics Letters B.

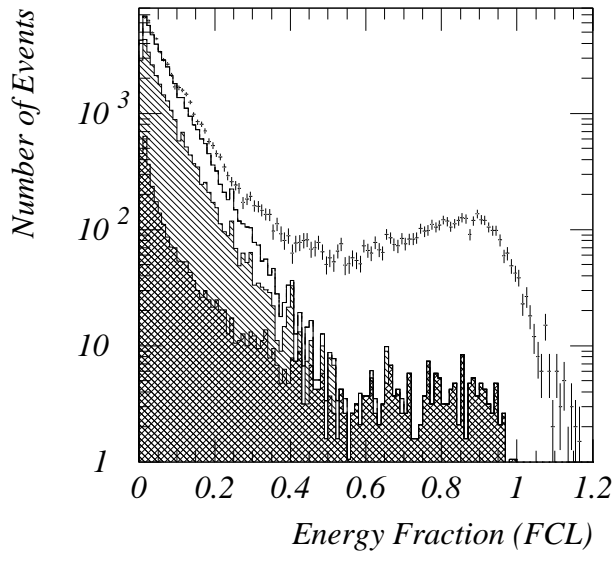


Figure 2, R. Enomoto et al., Physics Letters B.

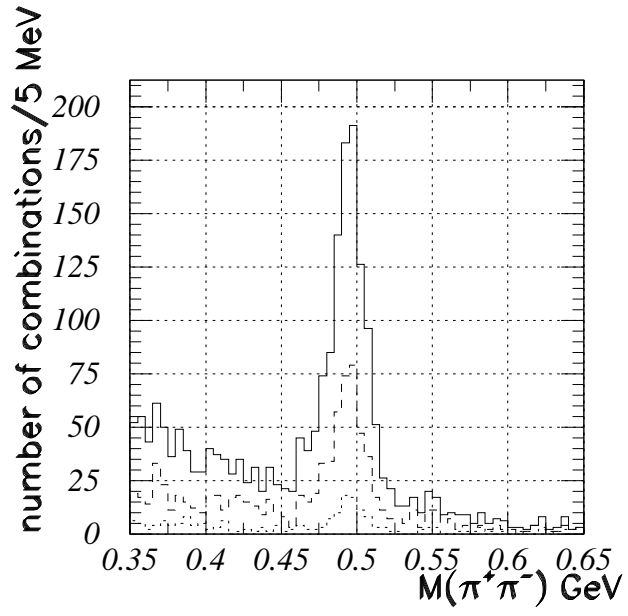


Figure 3, R. Enomoto et al., Physics Letters B.

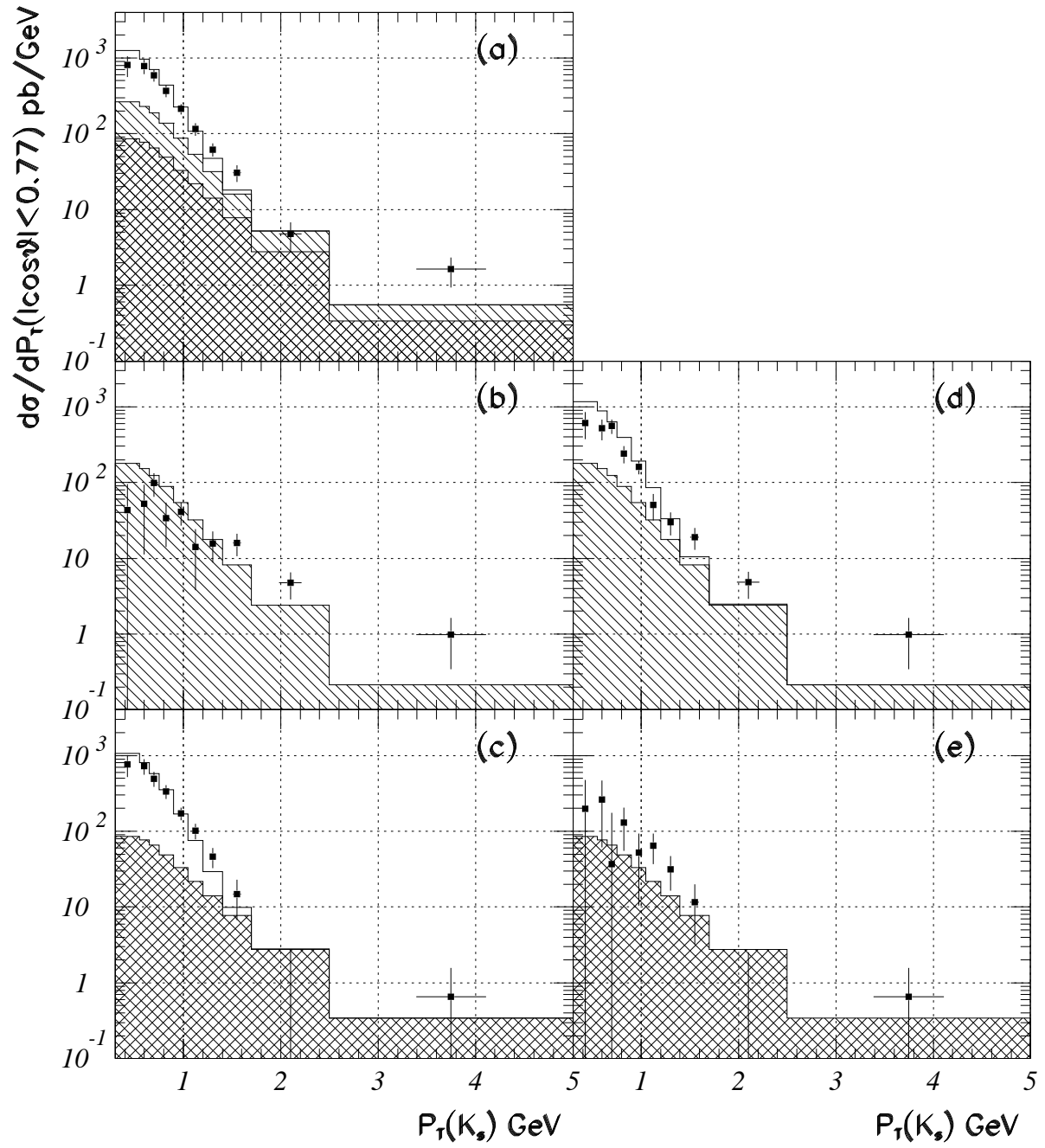


Figure 4, R. Enomoto et al., Physics Letters B.

